# Predictive capability of dc microplasma modeling in atmospheric pressure argon

M. Baeva, D. Loffhagen, M. M. Becker and D. Uhrlandt

*Leibniz Institute for Plasma Science and Technology, Greifswald, Germany*

**Abstract:** Numerical modeling of dc discharges in atmospheric pressure argon is performed by means of a spatially one-dimensional fluid model to study the impact of different approaches on the model's predictions. A comparison of various plasma parameters is given for a wide range of discharge currents in a parallel-plate arrangement with an inter-electrode gap of 0.4 mm. The behavior of the plasma parameters corresponding to various discharge regimes and the model's capability of a unified description of microarcs are discussed.

**Keywords:** direct current microplasma, glow to arc transition, one-dimensional modeling

## 1. Introduction

Small-scale plasmas (several hundred micrometer) generated by microdischarges in the glow regime have found numerous applications in the past two decades [1, 2]. Their main advantage is the stable operation at atmospheric pressure, which allows to reduce the cost of material processing and micro fabrication. Due to their low gas temperature, microdischarges have become attractive for plasma medicine. Glow microdischarges have been studied intensively by modeling [3-6] and diagnostics [7], which have given more insight into their physical parameters (gas temperature, electron density and energy). Studies on microarc plasmas can significantly contribute to their knowledge improvement and to the description of nonequilibrium regions in arc plasmas, which are widely used in technological applications. While the interest in nonequilibrium arc plasmas has grown during the last decade, experimental and theoretical studies on microarcs are still scarce. Some modeling studies are reported in [8,9]. They are based on a fluid approach and consider the conservation equations for charged and neutral species, the conservation of electron and heavy particles energy, and the Poisson equation. Although these studies have shown the transition from glow to arc regime of the microdischarge, the impact of the fluid description of the electron component with respect to the relationship of transport properties and rate coefficients to the mean electron energy has not been analyzed. Moreover, the heating of a thermionic cathode, which is essential for the sustainability of the microarc, was not treated in a self-consistent manner but by applying a given value of the voltage drop in the cathode sheath.

In this work, we present self-consistent modeling studies of microdischarge argon plasmas at atmospheric pressure under conditions corresponding to the glow and the arc regime as well as to the transition from glow to arc. We analyze the impact of various formulation of the electron transport properties on the discharge characteristics.

## 2. Physical background

A spatially one-dimensional model is considered (Fig. 1) to study a parallel-plate configuration of the discharge with an inter-electrode gap of 0.4 mm, which is much shorter than the radius of the electrodes (2 mm). The cathode body is included into the computational domain with a length of 20 mm. The electrodes are connected to a voltage source $U_0$ through a ballast resistor R to control the electric current in the discharge.

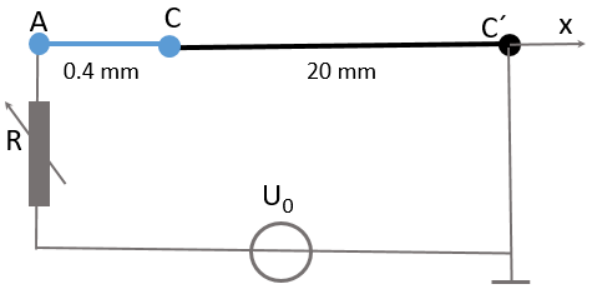


Fig. 1. Schematics of the electrodes and the external circuit: A – anode, C – cathode, x – coordinate axis.

The discharge is operated in argon at atmospheric pressure. The plasma-chemical model accounts for the reactions listed in **Table 1**, which occur between electrons (e), ground state argon atoms (Ar), a group of excited argon atoms ($Ar^*$), dimers ($Ar_2^*$), atomic ions ($Ar^+$), and molecular ions ($Ar_2^+$). The group $Ar^*$ includes the excited states of the 25-level system of M. Hayashi [10]. The rate coefficients (RC) are taken from published data or are obtained using published cross section (CS) data. In general, we use rate and transport coefficients for the electrons, which are obtained by solving their space-independent Boltzmann equation (BE) in a two-term expansion approach for given reduced electric field *E/N* and atomic data. Furthermore, a Maxwellian electron velocity distribution function (EVDF) is used for the sake of comparison.

The model of the microdischarge solves the equations of particle conservation for electrons, ions and excited species, the energy conservation of electrons and heavy particles, the Poisson equation for the electric potential *V*, the equation of heat transfer in the cathode made of tungsten and the electric circuit equation. Notice that the heat transfer in the cathode body is considered for the sake of a self-consistent coupling of the plasma to the electrode, which enables the description of the glow to arc transition.

Table 1. Processes considered in the model.

| | Reaction | Reference |
|---|---|---|
| 1 | e + Ar → e + Ar | CS [10] |
| 2 | e + Ar → e + Ar$^*$ | CS [10] |
| 3 | e + Ar$^*$ → e + Ar | CS [10] |
| 4 | e + Ar → 2e + Ar$^+$ | CS [10] |
| 5 | e + Ar$^*$ → 2e + Ar$^+$ | CS [11] |
| 6 | e + $Ar_2^*$ → 2e + $Ar_2^+$ | CS [12] |
| 7 | e + $Ar_2^*$ → e + 2Ar | CS [22] |
| 8 | e + $Ar_2^+$ → Ar$^*$ + Ar | RC [13] |
| 9 | e + $Ar_2^+$ → e + Ar$^+$ + Ar | RC [14] |
| 10 | 2e + Ar$^+$ → e + Ar | RC [15] |
| 11 | Ar$^*$ + Ar$^*$ → e + Ar$^+$+Ar | RC [16] |
| 12 | Ar$^*$ + Ar → Ar+Ar | RC [17] |
| 13 | 2$Ar_2^*$ → 2Ar + e + $Ar_2^+$ | RC [18] |
| 14 | 2Ar + Ar$^+$ → Ar + $Ar_2^+$ | RC [18] |
| 15 | 2Ar + Ar$^*$ → Ar + $Ar_2^*$ | RC [19] |
| 16 | Ar + $Ar_2^+$ → 2Ar + Ar$^+$ | RC [14] |
| 17 | Ar$^*$ → Ar + hν | RC[20,21] |
| 18 | $Ar_2^*$ → 2Ar +hν | RC[19] |

The corresponding equations read as follows:

$$\frac{\partial n_e}{\partial t} + \nabla \cdot \vec{\Gamma}_e = S_e, \tag{1}$$

$$\frac{\partial n_\varepsilon}{\partial t} + \nabla \cdot \vec{\Gamma}_\varepsilon + \vec{E} \cdot \vec{\Gamma}_e = S_\varepsilon - Q_h, \tag{2}$$

$$\rho \frac{\partial Y_k}{\partial t} + \nabla \cdot \vec{J}_k = S_k, \tag{3}$$

$$\nabla \cdot \vec{E} = \frac{\rho_q}{\varepsilon_0}; \ \vec{E} = -\nabla V. \tag{4}$$

In Eqs. (1)-(3), $n_e$, $n_\varepsilon$, $\rho$ and $Y_k$ denote the electron number density, the density of electron energy, the total mass density and the mass fraction of species of kind $k$. $S_e$, $S_k$ and $S_\varepsilon$ describe the gain/loss of electrons, heavy species $k$ and electron energy due to the inelastic plasma-chemical processes in **Table 1**, respectively, and $Q_h$ is the electron energy loss due to elastic collisions with argon. The mass flux $\vec{J}_k$ of species $k$ in (3) includes contributions due to mass diffusion and migration of charged species driven by the electrostatic field $\vec{E}$, determined by solving (4). The space charge density $\rho_q = e(n_{Ar+} + n_{Ar2+} - n_e)$ follows from the plasma chemistry of the model. The electron particle flux $\vec{\Gamma}_e$ and the electron energy flux $\vec{\Gamma}_\varepsilon$ in (1) and (2) are treated in drift-diffusion approximation. In addition to the common drift-diffusion approximation

$$\vec{\Gamma}_e = -\mu_e n_e \vec{E} - \nabla(n_e D_e); \vec{\Gamma}_\varepsilon = -\mu_\varepsilon n_\varepsilon \vec{E} - \nabla(n_\varepsilon D_\varepsilon) \tag{5}$$

with $\mu_e$, $\mu_\varepsilon$ and $D_e$, $D_\varepsilon$ representing the mobility and diffusivity of electrons and electron energy, respectively, an improved drift-diffusion approximation [23,24] is applied as well. The latter reads

$$\vec{\Gamma}_e = -\frac{e}{m_e \nu_e} n_e \vec{E} - \frac{1}{m_e \nu_e} \nabla(n_e(\xi_0 + \xi_2)),$$

$$\vec{\Gamma}_\varepsilon = -\frac{e}{m_e \widetilde{\nu_e}} n_\varepsilon \left(\frac{5}{3} + \frac{2}{3}\frac{\xi_2}{\xi_0}\right)\vec{E} - \frac{1}{m_e \widetilde{\nu_e}} \nabla\left(n_\varepsilon(\widetilde{\xi_0} + \widetilde{\xi_2})\right), \tag{6}$$

where the frequencies $\nu_e$ and $\widetilde{\nu_e}$ of momentum and energy flux dissipation and the transport coefficients $\xi_0, \xi_2, \widetilde{\xi_0}, \widetilde{\xi_2}$ are given as integrals over the isotropic part and the first two contributions to the anisotropy of the EVDF over the kinetic energy of the electrons, respectively [24].

According to the formulations (5) and (6), and the way to obtain the transport parameters and rate coefficients as functions of the mean electron energy $\bar{\varepsilon} = n_\varepsilon/n_e$, the following three study cases are considered:

1. Formulation (5); Maxwellian EVDF; $\mu_e = \frac{e}{m_e \nu_e}$, $D_e = \mu_e T_e$, $\mu_\varepsilon = \frac{5}{3}\mu_e$, $D_\varepsilon = \frac{5}{3} D_e$ with $\nu_e = \frac{R_e}{n_e}$ and $T_e = \frac{2}{3}\bar{\varepsilon}$. $R_e$ is the total reaction rate for electron collision processes.
2. Formulation (5); EVDF from solution of BE; $\mu_e$, $D_e$ and $\nu_e$ from the EVDF; $\mu_\varepsilon = \frac{5}{3}\mu_e$, $D_\varepsilon = \frac{5}{3} D_e$.
3. Formulation (6); EVDF from solution of BE; $\nu_e$, $\widetilde{\nu_e}$, $\xi_0, \xi_2, \widetilde{\xi_0}, \widetilde{\xi_2}$ from EVDF.

In case 2, the mobility and diffusivity of electron energy are expressed by the related particle transport coefficient applying a factor of 5/3. This simplification, which is generally valid only for a Maxwellian EVDF (case 1), is frequently used in fluid modeling studies for the sake of numerical stability. Case 3 does not include such simplification.

The conservation of heavy particles (neutral and ionic species) energy is written as

$$\rho C_p \frac{\partial T}{\partial t} + \nabla \cdot \vec{q} = Q_h + Q_{iJ}, \tag{7}$$

where $T$ is the heavy particle temperature, $C_p$ denotes the specific heat capacity at constant pressure, $\vec{q} = -\lambda \nabla T$ is the heat flux due to heat conduction with the heat conductivity $\lambda$, $Q_h$ represents the energy gain due to elastic collisions between electrons and heavy particles, and $Q_{iJ}$ is the Joule heating of the ions. In this work, pressure work and viscous dissipation are not considered.

While the anode is assumed to be at constant temperature, the heat conduction in the cathode body is taken into account. The corresponding equation reads

$$A_s \rho_s C_{ps} \frac{\partial T}{\partial t} + \nabla \cdot \overrightarrow{q_s} = 0, \tag{8}$$

where $\overrightarrow{q_s} = -A_s \lambda_s \nabla T$ and $A_s$, $\rho_s, C_{ps}$, $\lambda_s$ are the cross section area, mass density, specific heat capacity, and heat conductivity of the cathode material (tungsten), respectively. The cathode is heated through the heat load from the plasma. In addition to secondary electron emission caused by ion impact onto the cathode, electrons can be emitted due to field-enhanced thermo-emission so that the discharge can be sustained in the arc regime. The

cathode end, which is not in contact with the plasma, is assumed to be at constant temperature. The Joule heating of the cathode is neglected for the region of current considered in the present work.

The plasma model and the electric circuit are coupled by the discharge current and voltage. The variation of the ballast resistance R (Fig. 1) allows us to adjust the discharge current. All three cases of the model are realized on the computational platform COMSOL Multiphysics®.

## 3. Results and discussion

Fig. 2 shows the current-voltage characteristics obtained for the three cases concerning the formulation of the drift-diffusion approximation and the electron transport properties. In all approaches, the transition from normal glow discharge (gd) to abnormal glow discharge (agd) to arc discharge (ad) can be reproduced. The assumption of a Maxwellian EVDF (case 1) is likely to underestimate the voltage of glow discharges, for which the current density $j$ is below about $10^5$ A/m$^2$. The 5/3-relationship of the electron and electron energy transport parameters within the drift-diffusion approximation (case 2) has a weak impact on the discharge voltage at low current densities and provides values similar to those for case 3.

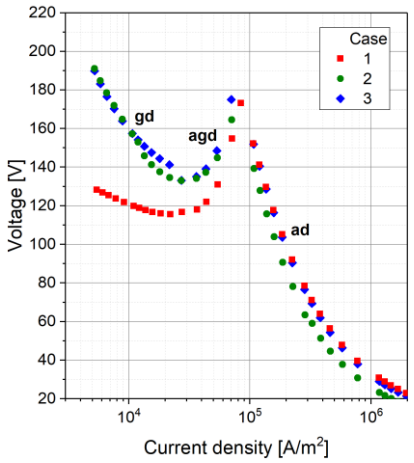


Fig. 2. *V-j* characteristics of the discharge obtained by the modeling approaches introduced as cases 1 to 3.

At current densities beyond ~ $1{\cdot}10^5$ A/m$^2$ and, in particular, in the arc regime of discharge, the voltage predicted by case 1 is close to that in case 3 so that a Maxwellian EVDF can be considered a reasonable choice for the microarc modeling.

In addition to the discharge voltage and current, the predictive capability of a discharge model includes the species densities, the mean electron energy, and the gas temperature among other plasma parameters. Fig. 3 shows plots of some plasma parameters obtained for cases 1-3 at current densities of about $5{\cdot}10^4$ A/m$^2$ and $5{\cdot}10^5$ A/m$^2$ (see Fig. 2). The spatial distribution of electron and ion densities in the gd-regime in case 1 deviates from the qualitatively similar behavior in cases 2 and 3. This is in contrast to the results in the ad-regime. The spatial distributions of the densities of excited atoms obtained for cases 2 and 3 are similar where the 5/3-simplification of the transport properties of the electron energy in case 2 leads to smaller values in the anode part of the plasma bulk. In the ad-regime, the behavior predicted by case 1 does not show the hill region in the bulk evident in case 3. The electron temperature (defined as 2/3 of the electron mean energy) obtained in case 3 undergoes a local minimum at the cathode sheath edge both in gd- and in ad-regime. The sharp increase of the electron temperature in the cathode sheath is more pronounced in the ad-regime. The result of case 2 significantly differs in the height of the peak reached in the cases 1 and 3. The gas heating is in general weakest in case 1 and strongest in case 3.

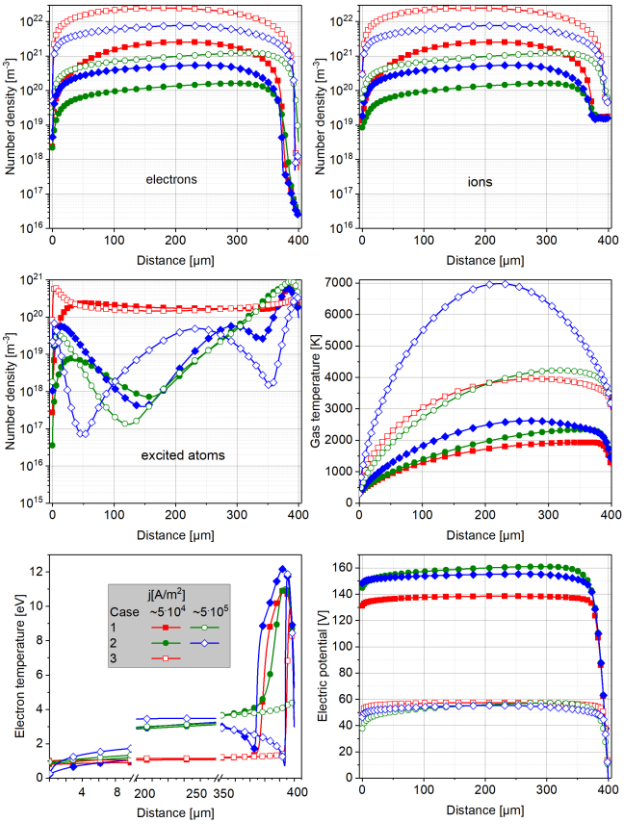


Fig. 3. Spatial distribution of various plasma parameters obtained for cases 1-3 at current densities of ~$5{\cdot}10^4$ A/m$^2$ (solid symbols) and ~$5{\cdot}10^5$ A/m$^2$ (open symbols).

Figures 4 shows the results for the particle densities obtained for case 3 in the gd-regime (solid symbols) and in ad-regime (open symbols). The end of the region of the quasi-neutral plasma bulk and the space-charge sheaths adjacent to the electrodes are plotted enlarged for better reading. The ion density corresponds to $n_{ion}=n_{Ar+}+n_{Ar2+}$. In the gd-regime, the electron and ion density reach maximum values of ~$5{\cdot}10^{20}$ m$^{-3}$ at a position closer to the cathode, while in the ad-regime, maximum values of ~$7{\cdot}10^{21}$ m$^{-3}$ are reached almost in the middle of the inter-electrode distance. The space-charge regions are positively

charged in both regimes and shorten by a factor of ~3 when the current density is increased by a factor of 10. The density of excited atoms shows in both regimes three local maxima. The highest one is in the cathode space-charge sheath, where the electron temperature rapidly increases (see Fig. 3) due to secondary (gd-regime) and emitted (gd-regime) electrons, that are accelerated by the strong electric field there. The second maximum in the spatial distribution of the excited atoms occurs at the position of maximum of the electron and ion density. The third maximum occurs close to the anode. This behavior is pronounced in less extend in cases 1 and 2 as it can be seen in Fig. 3.

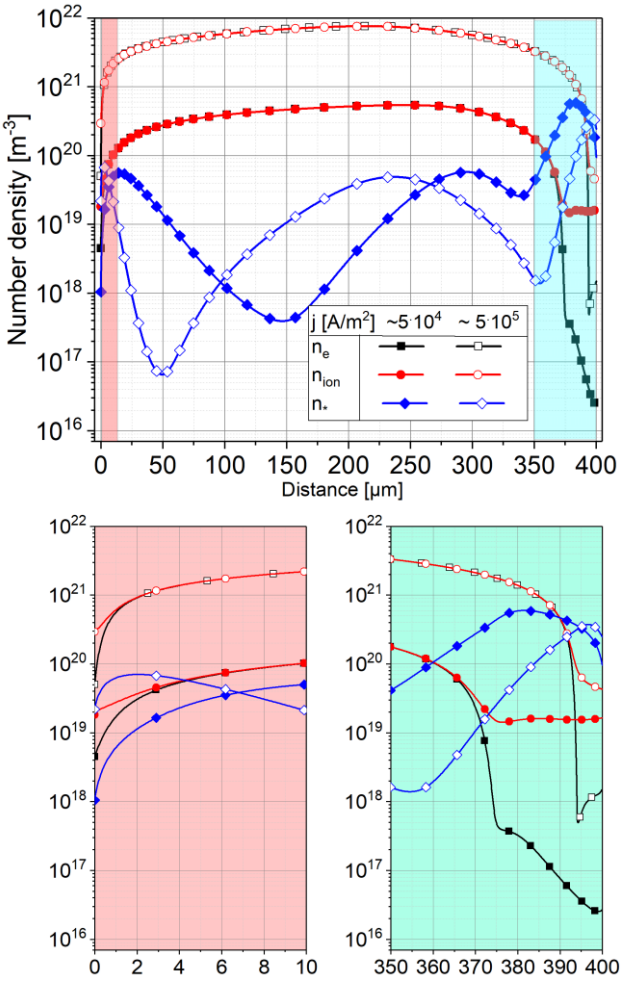


Fig. 4. Spatial distribution of particle densities obtained for case 3: electrons (squares), ions (circles) and excited atoms (diamonds) for current densities of ~5·10$^4$ A/m$^2$ (solid symbols) and ~5·10$^5$ A/m$^2$ (open symbols).

## 4. Conclusion

The present results of dc microplasma discharge modeling in argon at atmospheric pressure depend strongly on the assumptions concerning the description of the transport of electrons and their energy. A validation of the present results requires related measurements of voltage, particles densities and temperatures.

## 5. Acknowledgments

Funded by the Deutsche Forschungsgemeinschaft (DFG, German Research Foundation) - Project number 390828847.

## 6. References

[1] K. H. Schoenbach, K. Becker, Eur. Phys. J. D **70**, 29 (2016).
[2] K. Becker, K. H. Schoenbach, J. G. Eden, J. Phys. D: Appl. Phys. **39**, R55 (2006).
[3] D. B. Graves, K. F. Jensen, IEEE Trans. Plasma Sci. **14**, 78 (1986).
[4] M. J. Kushner, J. Phys. D: Appl. Phys. **38**, 1633 (2005).
[5] J.-P. Boeuf, L. C. Pitchford, K. H. Schoenbach, Appl. Phys. Lett. **86**, 071501 (2005).
[6] T. Farouk, B. Faraouk, A. Gutsol, A. Fridman, Plasma Sources Sci. Technol. **17**, 035015 (2008).
[7] P. Bruggeman, R. Brandenburg, J. Phys. D: Appl. Phys. **46**, 464001 (2013).
[8] S. I. Eliseev, A. A. Kudryavtsev, H. Liu, Z. Ning, D. Yu, A. S. Chirtsov, IEEE Trans. Plasma Sci. **44**, 2536 (2016).
[9] A. I. Saifutdinov, I. I. Fairushin, N. F. Kashapov, JETP Lett. **104**, 180 (2016).
[10] M. Hayashi, NIFS-DATA-72 Report (2003).
[11] L. Vriens, A. H. M. Smeets, Phys. Rev. A **22**, 940 (1980).
[12] M. R. Flannery, K. J. McCann, Technical Report AFWAL-TR-80-2015 (1980).
[13] A. J. Cunningham, T. F. O'Malley, R. M. Hobson, J. Phys. B: At. Mol. Phys. **14**, 773 (1981).
[14] J. Jonkers, M. van de Sande, A. Sola, A. Gamero, A. Rodero, J. van der Mullen, Plasma Sources Sci. Technol. **12**, 464 (2003).
[15] Y. P. Raizer, Gas Discharge Physics (Springer, 1991).
[16] N. B. Kolokolov, A. A. Kudrjavtsev, A. B. Blagoev, Phys. Scr. **50**, 371 (1994).
[17] D. P. Lymberopoulos, D. J. Economou, J. Appl. Phys. **73**, 3668 (1993).
[18] S. K. Lam, C.-E. Zheng, D. Lo, A. Dem'ynov, A. P. Napartovoch, J. Phys. D: Appl. Phys. **33**, 242 (2000).
[19] F. Kannari, M. Suda, M. Obara, T. Fujioka, IEEE J. Quantum Electron. **19**, 1587 (1983).
[20] T. Holstein, Phys. Rev. **72**, 1212 (1947)
[21] A. Kramida, Y. Ralchenko, J. Reader, NIST ASD Team, NIST Atomic Spectra Database.
[22] A. R. Hoskinson, J. Gregorio, S. Parsons, J. Hopwood, J. Appl. Phys. **117**, 163301 (2015).
[23] M. M. Becker, D. Loffhagen, AIP Adv. **3**, 012108 (2013).
[24] M. M. Becker, H. Kählert, A. Sun, M. Bonitz, D. Loffhagen, Plasma Sources Sci. Technol. **26**, 044001 (2017).